Rev. LatinAm. Metal. Mat.

Artículo Regular

www.rlmm.org

SYNTHESIS, CRYSTAL STRUCTURE AND MAGNETIC BEHAVIOR OF $CuCo_2InTe_4$ AND $CuNi_2InTe_4$

Pedro Grima-Gallardo[1,2], Miguel Soto[1], Orlando Izarra[1], Luis Nieves[1], Miguel Quintero[1], Gerzon E. Delgado[3], Humberto Cabrera[4,5], Inti Zumeta-Dubé[6], Alejandro Rodríguez[6], Jennifer R. Glenn[7] and Jennifer A. Aitken[7]*

1: Centro de Estudios en Semiconductores (C.E.S.). Departamento de Física, Facultad de Ciencias, Universidad de Los Andes, Mérida, Venezuela. ***2:*** Centro Nacional de Optica Avanzada (CNTO), Centro de Investigaciones en Astronomia (CIDA), Mérida, Venezuela. ***3:*** Laboratorio de Cristalografía, Departamento de Química, Facultad de Ciencias, Universidad de Los Andes, Mérida, Venezuela. ***4:*** International Centre for Theoretical Physics (ICTP), Trieste, Italy. ***5:*** Centro Multidisciplinario de Ciencias, Instituto Venezolano de Investigaciones Científicas (IVIC), Mérida, Venezuela. ***6:*** Centro de Investigación en Ciencia Aplicada y Tecnología Avanzada, Unidad Legaria, Instituto Politécnico Nacional, México. ***7:*** Department of Chemistry and Biochemistry, Duquesne University, Pittsburgh, Pennsylvania 15282, USA.

**e-mail: peg@ula.ve*

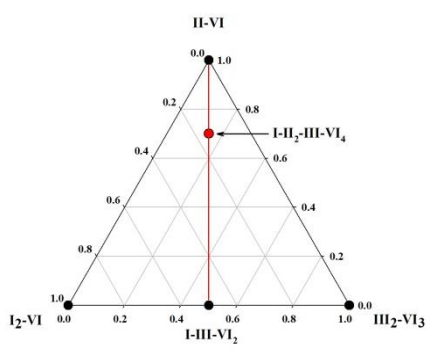

ABSTRACT

Polycrystalline samples of nominal $CuCo_2InTe_4$ and $CuNi_2InTe_4$ were prepared by the melt and anneal method and the products characterized by powder X-ray diffraction and SQUID techniques. It was found that $CuCo_2InTe_4$ and $CuNi_2InTe_4$ crystallize in the tetragonal space group (Nº 121), Z = 2, in a stannite-type structure, with the binaries CoTe and NiTe as secondary phases, respectively. The magnetic behavior of $CuCo_2InTe_4$ is that of a superparamagnetic state with an irreversibility temperature of ~450K and a maximum coercive field of 35 Oe at 2K; whereas $CuNi_2InTe_4$ shows two magnetic components, one diamagnetic an another weak ferromagnetic.

Keywords: $CuCo_2InTe_4$, $CuNi_2InTe_4$, x-ray diffraction, magnetism.

SÍNTESIS, ESTRUCTURA CRISTALINA Y COMPORTAMIENTO MAGNÉTICO DE $CuCo_2InTe_4$ Y $CuNi_2InTe_4$

RESUMEN

Se prepararon muestras policristalinas de $CuCo_2InTe_4$ and $CuNi_2InTe_4$ en su valor nominal por el método de fusión y recocido, y los productos fueron caracterizados por las técnicas de difracción de rayos X y SQUID. Se encontró que $CuCo_2InTe_4$ and $CuNi_2InTe_4$ cristalizan en una estructura tetragonal, grupo espacial (Nº 121), Z = 2, tipo estannita, con presencia de los binarios CoTe y NiTe como fases secundarias, respectivamente. El comportamiento magnético de $CuCo_2InTe_4$ es de tipo superparamagnético con una temperatura de irreversibilidad de ~450K y un campo coercitivo máximo de 35 Oe a 2K; mientras que $CuNi_2InTe_4$ presenta dos componentes magnéticas, una diamagnética y otra ferromagnética débil.

Palabras clave: $CuCo_2InTe_4$, $CuNi_2InTe_4$, difracción de rayos x, magnetismo.

1. INTRODUCTION

Diluted magnetic semiconductors (DMS) have been extensively investigated because of their peculiar magnetic and magneto-optical properties arising from the presence of magnetic ions in the lattice [1]. The DMS materials more frequently studied are solid solutions obtained from the tetrahedral coordinated derivatives of the II-VI semiconductor family [2]. One of these derivative families are the quaternary semiconductors with formula I-II_2-III-VI_4 which belong to the normal compound of fourth derivatives of the II-VI binary semiconductors with three types of cations [3], and fulfill the rules of adamantine compound formation [2-3]. According to these rules, the cation substitution is performed in such a way that an average number of four valence electrons per atomic site and a value eight for the ratio valence electrons to anions is maintained [2].

I-II_2-III-VI_4 materials are obtained from $(I\text{-}III\text{-}VI_2)_{1-x}$ $(II\text{-}VI)_x$ solid solutions system when x=2/3 (Figure 1, left side) or x=1/2 when the alternative expression $(I\text{-}III\text{-}VI_2)_{1-x}$ $2(II\text{-}VI)_x$ is used (Figure 1, right side). Both representations are equivalent, but some authors prefers the second one because is more explicit in the fact that it is necessary that a pair of I-III atoms are replaced by two II atoms in order to maintain the ratio of 4 valence electrons by atom.

In the early stage of the investigation on I-II_2-III-VI_4 materials, Zn or Cd was often used as an II-type atom for the substitution of I-III pair of atoms on $(I\text{-}III\text{-}VI_2)_{1-x}$ $(II\text{-}VI)_x$ solid solution systems. In the classic book of Shay and Wernick on chalcopyrite semiconductors (1974) [4] there is a list of twenty formulations of the general composition I-II_2-III-VI_4, which did not form ordered superstructures, but rather yielded simple diffraction patterns indicative of cubic zincblende (ex: $CuZn_2InSe_4$) or hexagonal wurzite (ex: $CuCd_2InS_4$) structures, where all three cations would exist disordered on the one crystallographic unique cation site in these structure types.

More recently, Chen *et al.* (2009) [5-6], by first-principle calculations obtained that, for I-II_2-III-VI_4 materials, three superstructures were also possible (Figure 2): Kesterite (KS) space group $I\bar{4}$, stannite (ST) space group $I\bar{4}2m$ and the mixed CuAu structure space group $P\bar{4}2m$. This calculation has been partially confirmed by experiments, in fact, it has been reported that $CuFe_2(Al,Ga,In)Se_4$ [7-8], $CuTa_2InTe_4$ [9], $AgFe_2GaTe_4$ [10] and the stable forms at higher temperatures of $CuZn_2(Al,Ga,In)S_4$ [11] crystalizes in the ST structure, whereas for $AgCd_2GaS_4$ [12], $AgCd_2GaSe_4$ [13], $Ag_{1-x}Cu_xCd_2GaS_4$ [14], $AgCd_2Ga_{1-x}In_xS_4$ [15] and $AgCd_{2-x}Mn_xGaS_4$ [16] a wurtz-stannite superstructure with orthorhombic space group $Pmn2_1$ (Nº 31) has been obtained.

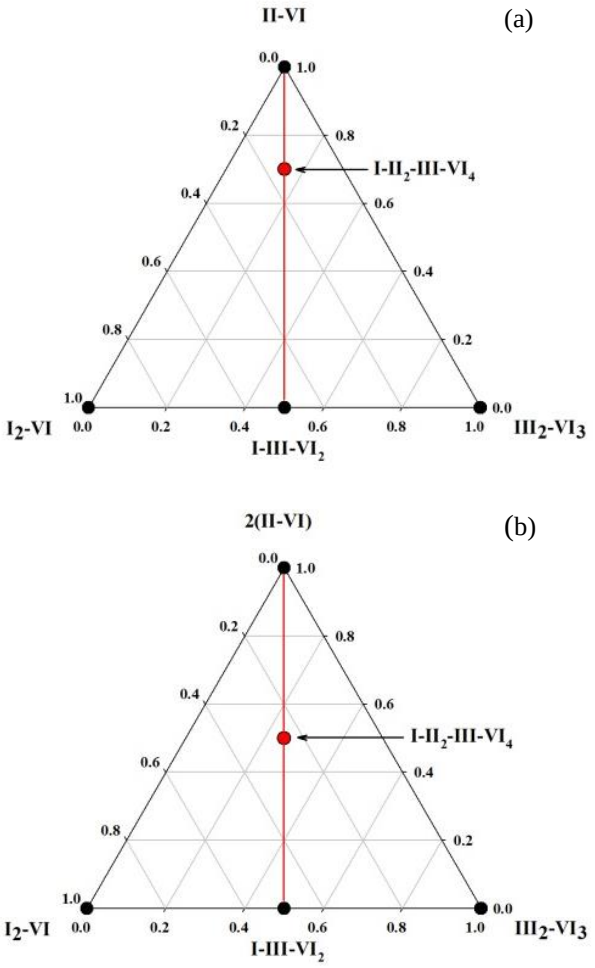

Figure 1. Equivalent representations of solid solutions systems: (a) $(I\text{-}III\text{-}VI_2)_{1-x}(II\text{-}VI)_x$ and (b) $(I\text{-}III\text{-}VI_2)_{1-x}$ $2(II\text{-}VI)_x$ and location of I-II_2-III-VI_4 materials (red point over the red line).

From the magnetic point of view, chalcopyrite materials (and based solid solutions) were extensively studied in the last decades of the twenty century due to their applications in solar cells. But, in the beginning of the twenty-one century, a renewed interest appears due to the discovery of room temperature ferromagnetism in these materials where doping with Mn [17]. Ferromagnetism in Mn-

substituted semiconductors is thought to arise from interaction of a hole with the local moment of the *d* electrons of Mn [18]. However, the solubility of Mn in chalcopyrite compounds is low, around 20% or less, which limits the production of holes. It is evident that the search will be extended to other transition metals (TM). Another magnetic state, superparamagnetic, was also observed in Mn-doped $CuGaTe_2$ [19-20] and $CuFe(Ga,In)Te_3$ [21] due to presence of magnetic clusters. These magnetic clusters, depending of the inter-cluster magnetic interactions can give place to: a) classic *superparamagnetism* as described by the Néel–Brown model when interactions are sufficiently weak, b) *superspin glass* (SSG) at sufficiently strong interactions, similar to those of atomic spin-glass systems in bulk, and c) *superferromagnetism* (SFM) when sufficiently strong interactions exist but they still below physical percolation. SFM domains in a non-percolated magnetic cluster assembly are expected to be similar to conventional ferromagnetic domains, with the decisive difference that the atomic spins are replaced by the *superspins* of the single-domain clusters [22].

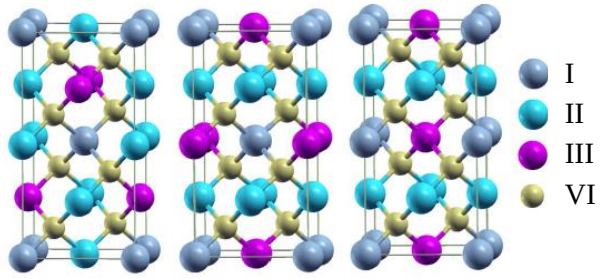

Figure 2. Three cell superstructures for $I\text{-}II_2\text{-}III\text{-}VI_4$ materials according to Chen et al (from the left to the right: KS, ST and mixed CuAu) [4-5].

As it was stated in previous paragraphs, crystal structures and magnetic behaviors are some of the many interesting subjects of investigation on $I\text{-}II_2\text{-}III\text{-}VI_4$ materials. The knowledge of their physical properties are crucial for their applications as absorbers in solar cells [5, 23], spin-polarized electron sources (SPES) [6] and spintronics (spin transistors, magnetic random access memories, etc) [24]. In this work, we report the crystal structure and magnetic behavior of nominal $CuCo_2InTe_4$ and $CuNi_2InTe_4$, derived from the $(CuInTe_2)_{1-x}(MT\text{-}Te)_x$ solid solutions with MT: Co or Ni and x = 2/3.

2. EXPERIMENTAL PROCEDURE

Preparation of the samples. Nominally $CuCo_2InSe_4$ and $CuNi_2InSe_4$ samples were synthesized using the melt-anneal method. Stoichiometric quantities of the elements with purity of at least 99.99% were charged in an evacuated synthetic silica glass ampoule, which was previously subjected to pyrolysis in order to avoid reaction of the starting materials with silica glass. Then, the ampoule was sealed under vacuum (~10^{-4} Torr) and the fusion process was carried out inside a furnace (vertical position) heated up to 1500K at a rate of 20K/h, with a stop of 48 h at 722.5K (melting temperature of Te) in order to maximize the formation of binary species at low temperature and minimize the presence of unreacted Te at high temperatures. The ampoule was shaken using a mechanical system during the entire heating process in order to aid the complete mixing of all the elements. The maximum temperature (1500K) was held for an additional 48 hours with the mechanical shaking system on. Then, the mechanical shaking system was turning off and the temperature was gradually lowered, at the same rate of 20K/h, until 873K. The ampoule was held at this temperature for a period of 30 days. Finally, the sample was cooled to room temperature at a rate of 10K/h. The obtained ingots were bright gray in color and homogeneous to the eye.

X-Ray Powder Diffraction. A small amount of each compound was thoroughly ground in an agate mortar and pestle. X-ray powder diffraction patterns were recorded using a PANalytical X'Pert Pro MPD powder X-ray diffractometer operating in Bragg-Brentano geometry using CuK_α radiation with an average wavelength of 1.54187 Å. A tube power of 45 kV and 40 mA was employed. A nickel filter was used in the diffracted beam optics and the data were collected with the X'Celerator one-dimensional silicon strip detector. A 0.25° divergent slit, a 0.5° antiscatter slit, and a 0.02 rad soller slit were set at both the incident and diffracted beams. The scan range was from 5 to 145° 2θ with a step size of 0.008° and a scan speed of 0.0106°/s.

SQUID measurements. DC measurements were performed on a Quantum Design SQUID magnetometer, equipped with a superconducting magnet able to produce fields up to 8 x 10^4 Oe. The samples in the form of powder were compacted with a piece of cotton inside the sample holder in order to

prevent any movement of the sample during measurements. Magnetic susceptibility measurements were performed using the Zero Field Cooling (ZFC)-Field Cooling (FC) protocol in the temperature range of 2–400K. ZFC consists of in cooling the sample from the highest temperature, to the lowest measuring temperature in a zero magnetic field; then a static magnetic field (100 Oe) is applied and magnetization measured during warming up. FC measurement consists of cooling the sample and measuring the magnetization during heating (at the same rate that in the ZFC process) without removal of the field. Magnetization as a function of the applied magnetic field at a given temperature measurements were also performed for magnetic fields in the range $-7x10^4 < H < 7x10^4$ Oe and temperatures of 1.8, 50, 150, 250 and 300K.

3. EXPERIMENTAL RESULTS AND DISCUSSION

Crystal structure. Figure 3 and 4 shows the resulting X-ray powder difractograms for nominal $CuCo_2InTe_4$ and $CuNi_2InTe_4$. An automatic search in the PDF-ICDD database [25], using the software available with the diffractometer, indicated that the powder patterns contained important amounts of the binaries CoTe (PDF N° 70-2887) and NiTe (PDF N° 89-2019), respectively.

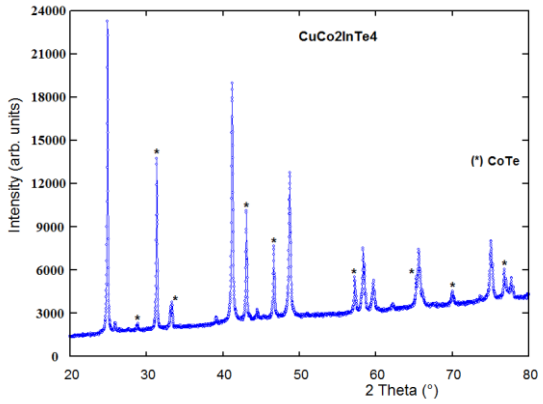

Figure 3. X-ray powder diffraction pattern of $CuCo_2InTe_4$. The CoTe (PDF 70-2887) secondary phase is denoted by asterisks.

The 20 first peak positions of the main phase, in each case, were indexed using the program Dicvol04 [26], which gave a unique solution in tetragonal cells with a = 6.195(2) Å, c = 12.400(4) Å for $CuCo_2InTe_4$ and a = 6.160(2) Å, c = 12.365(4) Å for $CuNi_2InTe_4$.

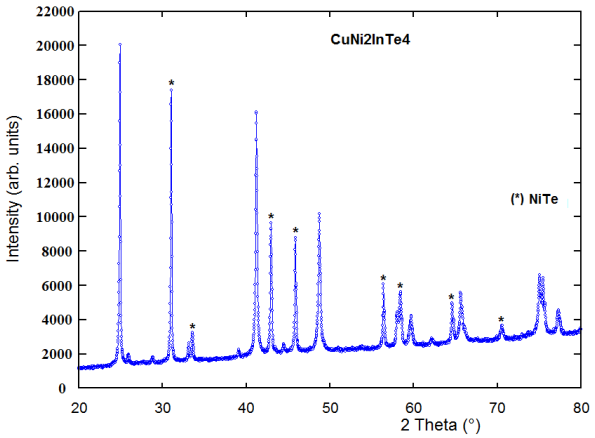

Figure 4. X-ray powder diffraction pattern of $CuNi_2InTe_4$. The NiTe (PDF 89-2019) secondary phase is denoted by asterisks.

The systematic absences study (hkl: h + k + l = 2n) indicated an I-type cell. A revision of the diffraction lines of the main phase taking into account the sample composition, unit cell parameters as well as the body center cell suggest that this material is isostructural with $CuFe_2InSe_4$ [7] and $AgFe_2GaTe_4$ [10]; the firsts compounds of the I-II_2-III-VI_4 family with a stannite structure [27], which crystallize in the tetragonal space group $I\bar{4}2m$ (Nº 121). The Rietveld refinement [28] of the whole diffraction patterns was carried out using the Fullprof program [29], with the unit cell parameters mentioned above (see figure 5).

Atomic coordinates of the compound $CuFe_2InSe_4$ [13] were used as initial model for the refinements, with the cation distribution shown in Tables I and II. Atomic positions of the CoTe [30] and NiTe [31] binaries were included as secondary phases in the refinements. Atomic coordinates, isotropic temperature factor, bond distances and angles are shown in Tables 1 and 2.

It should be mentioned that Rietveld refinement were performed in the $I\bar{4}$ (N° 82) space group but did not produce a chemically sound structures, discarding kesterite structures. However, similar calculations using the $I\bar{4}2d$ space group for the tetragonal phase give also relative good figure of merit than for $I\bar{4}2m$, in consequence a physical discussion is necessary. In the chalcopyrite structure (s.g. $I\bar{4}2d$) the cationic sublattice is ordered, i.e. The VI-anion is surrounded by four cations, two of the group I and two of the group III. When a

chalcopyrite compound is doped (or alloyed) with a different II^{2+}-atom, this atom occupies a crystallographic site in the cationic sublattice creating disorder. This accumulative disorder that increase with the amount of the doped material can be observed in the investigation of the solid solutions, as it is the case of the recently reported $(CuInSe_2)_{1-x}(FeSe)_x$ [32].

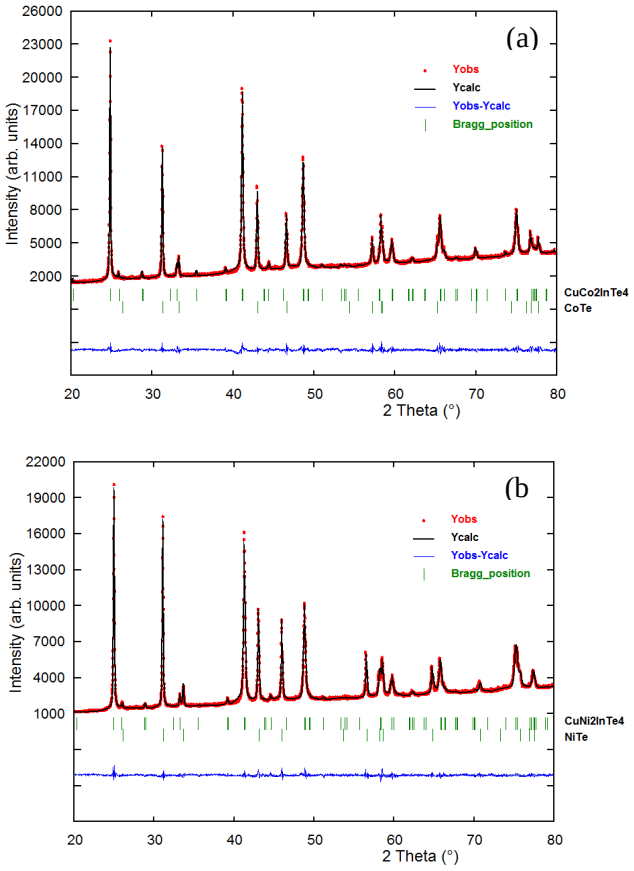

Figure 5. Final Rietveld plot showing the observed, calculated and difference pattern for (a) $CuCo_2InTe_4$ and (b) $CuNi_2InTe_4$. The Bragg reflections for both phases are indicated by vertical bars.

In this work we hypothesized the following crystal evolution (see figure 6): the ordered tetragonal chalcopyrite α-phase, space group $I\bar{4}2d$ transits to a semi-ordered chalcopyrite-like α´-phase, space group $P\bar{4}2c$, in the interval $0 < x < 2/3$, and then goes to a re-ordered stannite δ-phase, space group $I\bar{4}2m$, at $x = 2/3$. The behavior could be more complicated. Recently we have observed a reordering of the cationic sublattice at x=0.5 in the $(CuInTe_2)_{1-x}(FeTe)_x$ solid solution system [33].

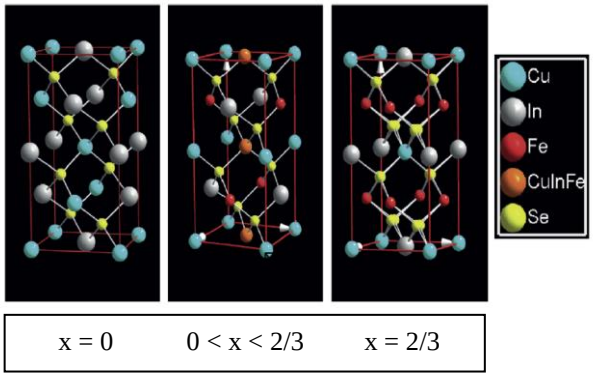

Figure 6. Evolution of the crystal structure of the $(CuInSe_2)_{1-x}$ $(FeSe)_x$ solid solution system with composition *x*. Left: $x = 0$, phase α (ordered tetragonal chalcopyrite) space group $I\bar{4}2d$; center: $x = 0.5$, phase α' (semi-ordered tetragonal chalcopyrite-like) space group $P\bar{4}2c$; right: $x = 2/3$, phase δ (ordered stannite) space group $I\bar{4}2m$. The orange atom (only in the crystal structure at the center of the figure) is labeled *CuInFe* because this crystallographic site is shared at random by the three cations *Cu*, *In* or *Fe*. For the representation of the $(CuInTe_2)_{1-x}$ $((Co/Ni)Te)_x$ solid solution systems the *Se*-atom must be changed for *Te*.

What is certain, is that the field of the ordered chalcopyrite α-phase in the I-III-VI_2 / II-VI alloys is limited to x ~ 0.25 [34] and the possibility of the existence of this phase at x = 2/3 is very improbable. Experimentally, the observed diffraction patterns correspond to a 65.3/34.7 proportion for $CuInTe_2$/CoTe and 58.3/41.7 for $CuInTe_2$/NiTe, values which are very different to the nominal proportion 33.33/66.66 which correspond to x=2/3. This result indicates that large amounts of Co and Ni have been diluted in the tetragonal phase. Moreover, $CuInTe_2$ is a diamagnetic material with a negative magnetic susceptibility, but this parameter is positive for $Cu(Co,Ni)_2InTe_4$ materials as we will see in the next section. There no doubt that the cationic sublattice of $Cu(Co,Ni)_2InTe_4$ materials is occupied by Cu, In and Co (or Ni). The question to be answered is how ordered are they? And how it is possible to distinguish unambiguously chalcopyrite and stannite structures? The diffraction patterns of chalcopyrite and stannite structures are slightly different, only a few weak lines at low θ appears for the stannite, but it is necessary to have good ordered samples. For polycrystalline samples it not always clearly visible. Another interesting method to observe the order in the sample is using optical

absorption techniques [33], since the absorption curves of disordered samples show a broad impurity band previous to the direct band-gap transition; this broad band nearly disappears for ordered samples. In the next future, we will prepare the entire families $CuInTe_2$/CoTe and $CuInTe_2$/NiTe and optical measurements will be performed. These measurements will give us a better vision about the evolution of the crystallographic structure as a function of composition.

Table 1. Rietveld refinement results for $Cu(Co,Ni)_2InTe_4$ and (Co,Ni)Te.

	$CuCo_2InTe_4$	**CoTe**	**R (%)**	**$CuNi_2InTe_4$**	**NiTe**	**R (%)**
Molecular weight (g/mol)	806.63	186.53		806.15	186.29	
a (Å)	6.1997(1)	3.8939(1)		6.1669(1)	3.9411(2)	
c (Å)	12.380(1)	5.3728(2)		12.370(1)	5.3177(3)	
V (Å^3)	475.84(4)	70.55(1)		470.44(4)	71.53(1)	
System	tetragonal	hexagonal		tetragonal	hexagonal	
Space group	*I-42m* (N° 121)	*P6$_3$/mmm* (Nº 194)		*I-42m* (N° 121)	*P6$_3$/mmm* (Nº 194)	
Z	2	2	R_{exp}= 6.7	2	2	R_{exp} = 6.5
D_{calc} (g/cm^{-3})	5.63		R_p= 7.2	5.69		R_p= 7.2
Weight fraction (%)	65.3	34.7	R_{wp}= 9.5	58.3	41.7	R_{wp}= 9.6
R_B (%)	8.5	7.9	S = 1.4	8.7	8.0	S = 1.5

Table 2. Unit cell, atomic coordinates, isotropic temperature factor and selected geometric parameters (Å, °) for $Cu(Co/Ni)_2InTe_4$.

Atom	**Ox.**	**Wyck.**	***x***	***y***	***z***	**Foc**	**B (Å^2)**
Cu	+1	2*a*	0	0	0	1	0.31/0.23
Co/Ni	+2	4*d*	0	½	¼	1	0.31/0.23
In	+3	*2b*	0	0	½	1	0.31/0.23
Te	-2	8*i*	0.264/0.264	0.264/0.264	0.124/0.124	1	0.31/0.23

Cu-Te^{i}	2.577/2.575		Co–Te Ni-Te	2.694 2.677		In-Te	2.778/2.774	
Te-Cu-Te^{ii}	106.9/106.2	x4	Te-Co-Te^{iv}	109.6/109.5	x4	Te^{i}-In-Te^{iv}	107.8/108.1	x4
Te-Cu-Te^{iii}	110.6/111.2	x2	Te-Co-Te^{v}	109.2/109.4	x2	Te^{iv}-In-Te^{vi}	112.7/112.2	x2

Symmetry codes: (i) -0.5+x, -0.5+y, 0.5+z; (ii) -y, x, -z; (iii) -x, -y, z; (iv) -0.5+y, 0.5-x, 0.5-z; (v) -x, 1-y, z; (vi) 0.5-y, -0.5+x, 0.5-z

SQUID measurements. In Figure 7 (left side) the magnetic susceptibility of $CuCo_2InTe_4$ with an applied magnetic field of 60 Oe is displayed. Also, at the right side, the magnetic susceptibility of CoTe is also showed for comparison (in this figure, QA means sample prepared in quartz Ampoule and HP means sample prepared at high pressure) [35].

With respect to the influence of the secondary phase in our experimental curve, it can be observed that the magnetic susceptibility of CoTe is nearly constant in the entire measured temperature range, and his value is almost ten times lower than the minimal vale observed for $CuCo_2InTe_4$, then it can be considered than his effect only displaces our curve up horizontally by a very low value and do not affects at all the shape of the ZFC or FC curves.

The behavior of the magnetic susceptibility of $CuCo_2InTe_4$ is typical of a superparamagnetic state with an irreversibility temperature (T_{irr}) higher than the maximum temperature reached in the experiment (400K). In superparamagnetic (SPM) systems, χ_{ZFC} usually vanishes at very low temperature and increases gradually with increasing temperature up to the blocking temperature T_B because of the thermally activated alignment of the superspins along the magnetic field direction. Above T_B, however, the thermal energy destroys the alignment of the superspins in favor of SPM randomization. This leads to a gradual decrease in χ_{ZFC} with increasing temperature. However, in our curve, we observe a monotonic increase of χ_{ZFC} indicative that T_B has not reached yet (T_B > 400K).

An approximation to the blocking temperature value can be obtained from the difference between the susceptibilities FC and ZFC, given in figure 8. As it can be seen in this figure, the experimental values can be divided in two sets which can be interpreted as two different magnetic regimes. The blocking temperature (T_B) is the intersection with the temperature axis where χ_{FC}-χ_{ZFC} = 0 and gives a value of ~450K.

With respect to the FC curve, it increases with temperature with minimum values at very low temperatures. This behavior suggests a SSG state since the crossover from blocked-to-free or frozen-to-free superspin rotation, respectively, is marked by a peak with a rounded shape. Therefore, in order to decide on blocked SPM or SSG behavior more sophisticated data sets must be examined such as the complex ac susceptibility or magnetization after ageing and rejuvenation protocols [22].

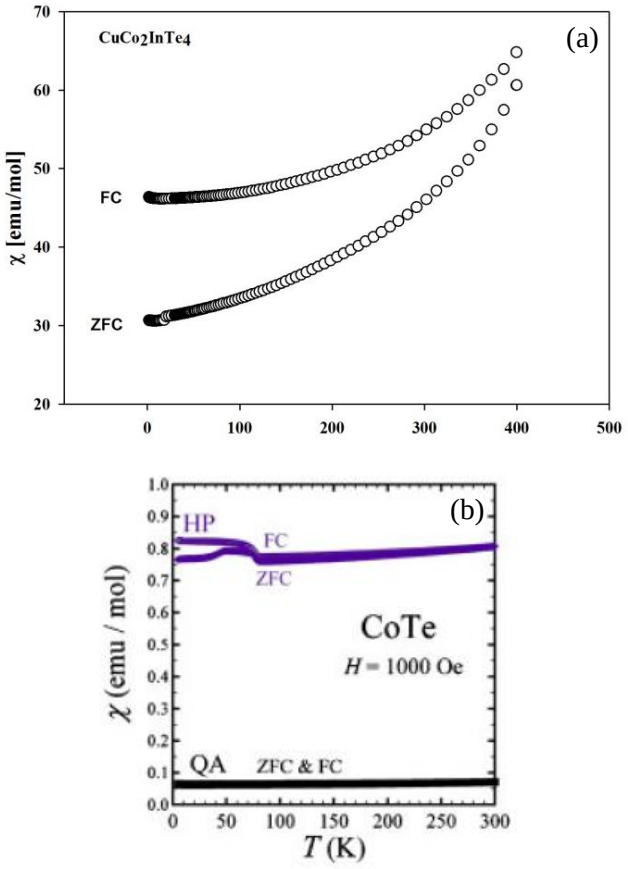

Figure 7. DC magnetic susceptibility of (a) $CuCo_2InTe_4$ and (b) CoTe [35].

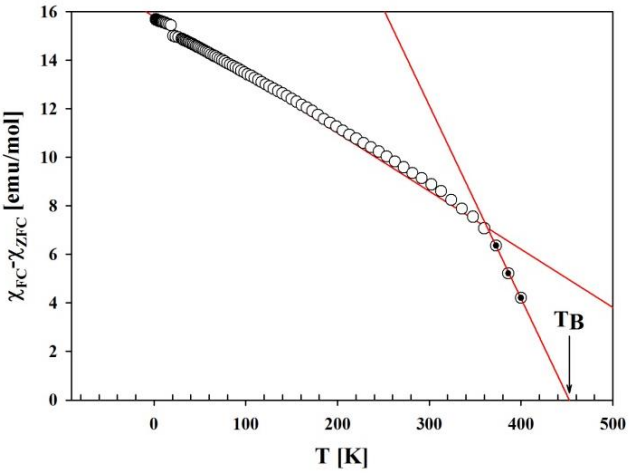

Figure 8. Difference between the susceptibilities FC and ZFC for $CuCo_2InTe_4$. The red lines are linear fits, one using all the experimental points and the other using only the three points at higher temperatures (white points with a littler black point).

The magnetization as a function of the applied field has been measured at 1.8, 50, 100, 250 and 300K in the range of $7x10^4 < H < 7x10^4$ Oe. In Figure 9, the results for 1.8 and 300K are shown.

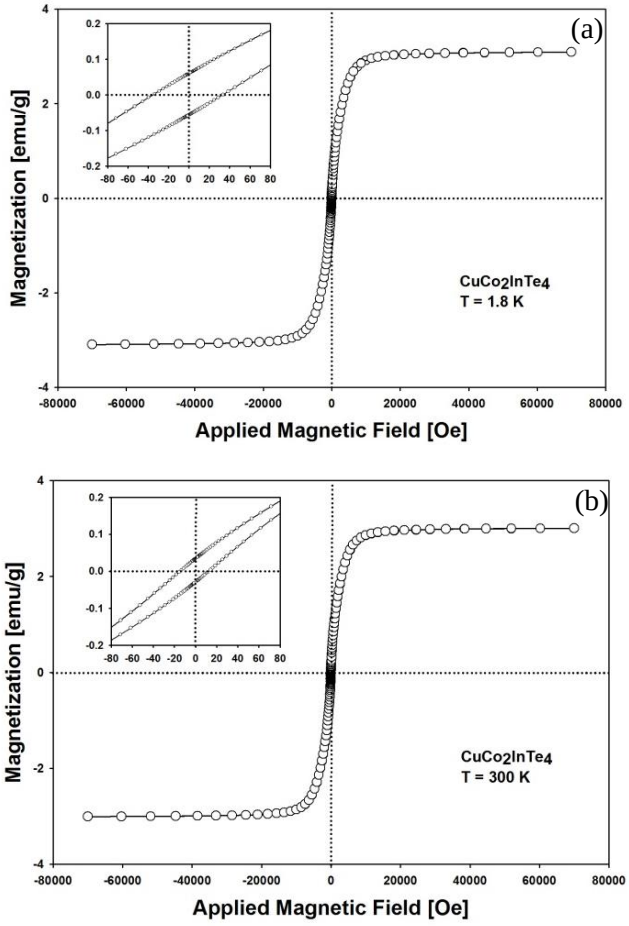

Figure 9. Magnetization as a function of the applied magnetic field, at (a) T=1.8K and (b) 300K for $CuCo_2InTe_4$. The inserts are an amplification of the low magnetic field region in order to clearly observe the respective magnetic hysteresis.

The relation between magnetic saturation (M_s) and residual magnetization (M_r) are 0.019 and 0.012 for T=1.8K and T=300K, respectively, indicating than $CuCo_2InTe_4$ is a very soft magnet.

The variation of the coercitive field (H_c) with temperature, it is given in figure 10. The experimental points have been fitted with the classical equation for a system of non-interacting and randomly oriented particles:

$$H_c = H_0\left(1 - \frac{T}{T_B}\right)^n \quad (1)$$

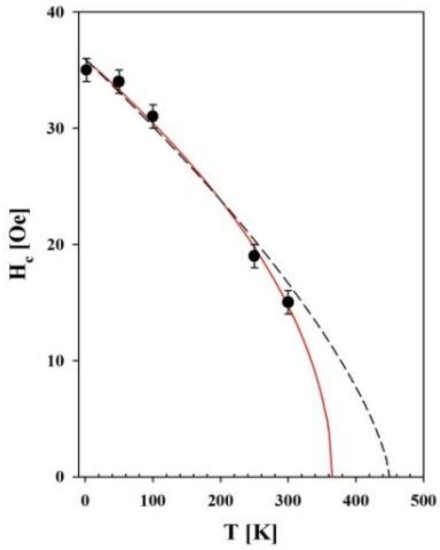

Figure 10. The coercitive field (H_c) as a function of temperature for $CuCo_2InTe_4$. The red line is a free fit with equation (1). The dashed line is a fit with the same equation but with T_B fixed at 450K.

Where H_0 is the coercitive field at $T_0 = 0K$, T_B is the blocking temperature and n must be close to 0.5. The free fit is the red line in Figure 8, that gives $H_0 = 35.94$ Oe, $T_B = 365K$ and n=0.52. Although the fit reproduces well the experimental points it does not give a reliable value for T_B. Instead the dashed line is a fit where the T_B temperature was fixed with the value obtained from figure 4 and gives H_0=35.94 Oe and n = 0.70. This last fit seems to have more physical meaning since a higher value of n implies more strong interactions between particles as there are in a SSG system suggested for the behavior of the FC curve.

In Figure 11, the DC magnetic susceptibility for $CuNi_2InTe_4$ is given (a) together with the reported analogous curve for NiTe [35].

The behavior of the magnetic susceptibility of the secondary phase (NiTe-QA) is similar to those of CoTe phase in the sense that it has a nearly constant value (~0.5 $x10^{-3}$ emu/mol) with temperature but shows a little hysteresis for T<180K. The presence of this secondary phase may be explain the relative high value of the diamagnetic component observed in $CuNi_2InTe_4$ but it seems not enough for the sharply increase of the $CuNi_2InTe_4$ curve at low temperatures.

The $CuNi_2InTe_4$ can be interpreted with the overlap of two magnetic components, one diamagnetic and

the other ferromagnetic. This interpretation is clearer if we observe the M Vs H curves (Figure 12). At very low temperature (1.8K) the weak ferromagnetic and the diamagnetic components coexists. The first one dominates at low magnetic field values whereas the second one dominates at higher magnetic field values. At T > 1.8K only the diamagnetic component is observed coherently with figure 11.

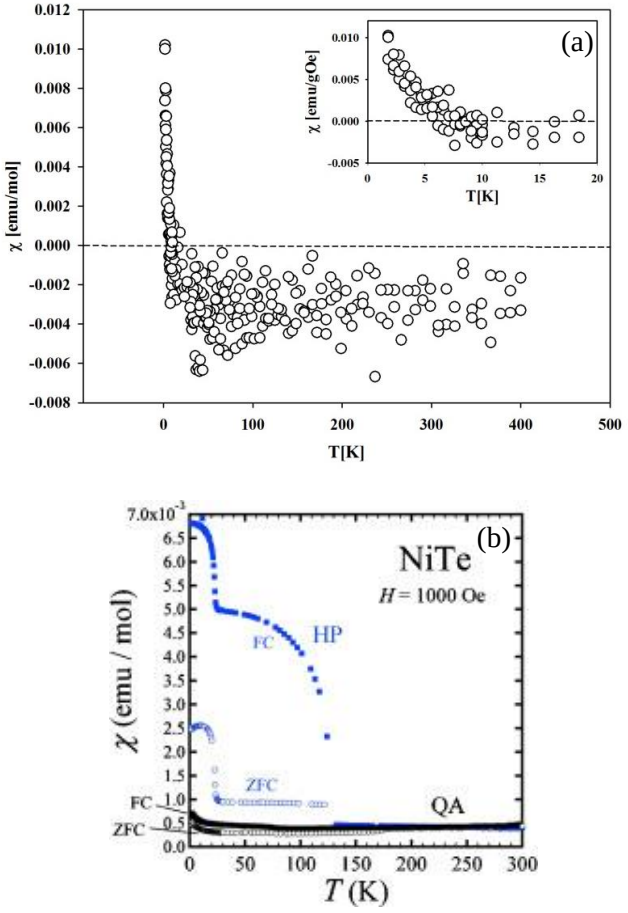

Figure 11. DC magnetic susceptibility of (a) $CuNi_2InTe_4$ and (b) NiTe [35].

4. CONCLUSIONS

The crystal structure and magnetic behavior of $CuCo_2InTe_4$ and $CuNi_2InTe_4$ have been investigated by XRD and SQUID techniques. It was found that both materials crystallizes in a tetragonal $I\bar{4}2m$ (Nº 121) with important amounts of a secondary phase (CoTe and NiTe, respectively). The magnetic behavior of $CuCo_2InTe_4$ is that of a superparamagnetic with a blocking temperature of ~450K whereas for $CuNi_2InTe_4$ we observed the presence of two superimposed magnetic components, one weak ferromagnetic and another diamagnetic.

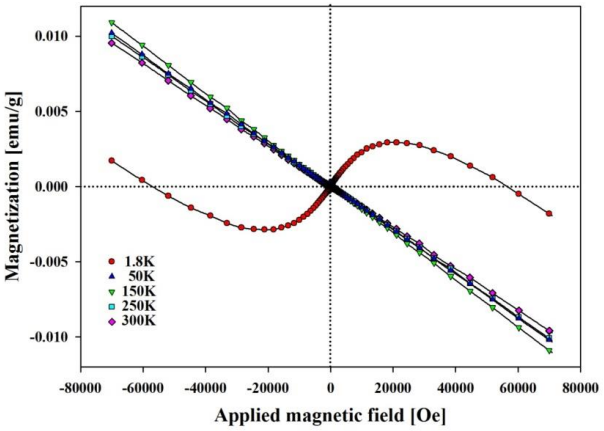

Figure 12. Magnetization Vs applied magnetic field curves for $CuNi_2InTe_4$ at 1.8, 50, 150, 250 and 300K.

5. ACKNOWLEDGEMENT

P.G-G wants to thank to CDCHTA-ULA grant code C-1885-14-05-B and Fondo Nacional de Ciencia, Tecnología e Innovación (FONACIT) project number 2011001341 (Fabricación de celdas solares fotovoltaicas de bajo costo mediante las técnicas combinadas de deposición electroquímica y evaporación). I.Z-D acknowledges postdoctoral fellow from CONACyT Project number CB2014-235840 (Desarrollo de Materiales para Tecnologías de Hidrógeno).

6. REFERENCES

[1]. Nikiforov K.G., Progr. Crystal Growth Charac. Mater. 1999; 39:1.

[2]. Parthé E., in : J.H. Westbrook, R.L. Fleischer (Eds.), Intermetallic compounds, principles and applications, Vol. 1, Jhon Wiley & Sons, Chichester, UK, Chap. 14. (1995).

[3]. Delgado J.M., Inst. Phys. Conf. Series 1998; 152:147.

[4]. Shay J.L. and Wernick J.H., "Ternary Chalcopyrite Semiconductors: Growth, Electronic Properties, and Applications", Pergamon Press, Oxford 1974.

[5]. Chen S., Gong X.G., Walsh A., Wei S.H., Phys. Rev. 2009; B79: 165211.

[6]. Chen S., Yin W.J., Yang J.H., Gong X.G., Wei S.H., Appl. Phys. Lett. 2009; 95: 052102.

[7]. Delgado G.E., Mora A.J., Grima-Gallardo P., Muñoz M., Durán S. and Quintero M., Phys. B:

Cond. Matter 2008; 403:3228.

[8]. Delgado G.E., Mora A.J., Grima-Gallardo P., Muñoz M., Durán S. and Quintero M., Mater. Res. Bull. 2014; 38:1061.

[9]. Delgado G.E., Mora A.J., Grima-Gallardo P., Muñoz M., Durán S. and Quintero M., Physica B 2008; 403:3228.

[10]. Delgado G.E., Quintero E., Tovar R., Grima-Gallardo P. and Quintero M., J. Alloys Comp. 2014; 613:143.

[11]. Ghosh A., Palchoudhury S., Thangavel R., Zhou Z., Naghibolashrafi N., Ramasamy K. and Gupta A., Chem. Comm. 2015. Accepted.

[12]. Chykhrij S.I., Parasyuk O.V. and Halka O.V., J. Alloys Comp. 2000, 312:189.

[13]. Olekseyuk I.D., Gulay L.D., Parasyuk O.V., Husak O. and Kadykalo E.M., J. Alloys Comp. 2002; 343:125.

[14]. Zmiy O.F., Mishchenko I.A. and Olekseyuk I.D., J. Alloys Comp. 2004; 367:49.

[15]. Olekseyuk I.D., Parasyuk O.V., Husak O., Piskach L.V., Volkov S.V. and Pekhnyo V.I., J. Alloys Comp. 2005; 402:186.

[16]. Davydyuk G.Y., Sachanyuk V.P., Voronyuk S.V., Olekseyuk I.D., Romanyuk Y.E., and Parasyuk O.V., Phys. B: Cond. Matter. 2006; 373:355.

[17]. Uchitomi N., Asubar J.T., Oomae H., Endoh H. and Jinbo Y.. J. Surf. Sci. Nanotech. 2011; 9: 95-102 and references there in.

[18]. Zhao Y-J. and Zunger A.. Phys. Rev. B 2004; 69: 104422 and references there in.

[19]. Novotortsev V. M., Shabunina G.G., Koroleva L.I., Aminov T.G., Demin R.V. and Boichuk S.V. Inorganic Materials 2007; 43: 12-17.

[20]. Pérez J., Silva P.J., Durante-Rincón C.A., Primera Ferrer J. and Fermin J.R. J. Magnetism and Magnetic Materials 2008; 320: 2155-2158.

[21]. Grima-Gallardo P., Alvarado F., Muñoz M., Durán S., Quintero M., Nieves L., Quintero E., Tovar R., Morocoima M. and Ramos M.A. Phys. Stat. Sol. A 2012; 209:1141-1143.

[22]. Bedanta S. and Kleemann W. J. Phys. D: Appl. Phys. 2009; 42:013001.

[23]. Walsh A., Wei Su-H., Chen S. and Gong X.G. Proceedings of the 34th IEEE Photovoltaic Specialists Conference 2009, Philadelphia, PA, USA.

[24]. Medina S., Bouhafs B. and Ruterana P. Computational Materials Science 2014; 85:159-163.

[25]. PDF-ICDD-Powder Diffraction File (Set 1-65), International Centre for Diffraction Data, 12 Campus Boulevard, Newtown Square, PA, USA (2013).

[26]. Boultif A. and Löuer D., J. Appl. Cryst. 2004; 37:724.

[27]. Hall S.R., Szymanski J.T. and Stewart J.M., Can. Mineral. 1978; 16:131.

[28]. Rietveld H. M. J. Appl. Cryst. 1969; 2:65.

[29]. J. Rodriguez-Carvajal, Physica B. 1993; 192:55.

[30]. de Meester de Betzembroeck P., and Naud J. Bull. Soc. Chim. Belg. 1971; 80:107.

[31]. Rost E., and Vestersjoe E., Acta Chem. Scand. 1968 ; 22:2118.

[32]. Grima-Gallardo P., Torres S., Quintero M., Nieves L., Moreno E. and Delgado G.E. J. Alloys and Compounds 2015; 630: 146-150.

[33]. P. Grima-Gallardo, M. Quintero, L. Nieves, H. Cabrera, E. Perez-Cappe, I. Zumeta-Dubé, J.A. Aitken and J.A. Brant. Submitted to RLMM Agost 2016.

[34]. Grima-Gallardo P. Phys. Stat. Sol. (a) 1992; 134:119.

[35]. Umeyama N., Tokumoto M, Yagi S., Tomura M., Tokiwa K., Fujii T., Toda R., Miyakawa N. and Ikeda S.-I. Jap. J. Appl. Phys. 2012; 51:053001.